

Pion scalar, vector, and tensor form factors from a contact interactionXiaobin Wang¹, Zanbin Xing¹, Jiayin Kang¹, Khépani Raya^{2,*} and Lei Chang^{1,†}¹*School of Physics, Nankai University, Tianjin 300071, China*²*Department of Integrated Sciences and Center for Advanced Studies in Physics, Mathematics and Computation, University of Huelva, E-21071 Huelva, Spain*

(Received 9 July 2022; accepted 24 August 2022; published 15 September 2022)

The pion scalar, vector, and tensor form factors are calculated within a symmetry-preserving contact interaction model (CI) of quantum chromodynamics (QCD), encompassed within a Dyson-Schwinger and Bethe-Salpeter equations approach. In addition to the traditional rainbow-ladder truncation, a modified interaction kernel for the Bethe-Salpeter equation is adopted. The implemented kernel preserves the vector and axial-vector Ward-Takahashi identities, while also providing additional freedom. Consequently, new tensor structures are generated in the corresponding interaction vertices, shifting the location of the mass poles appearing in the quark-photon and quark tensor vertex and yielding a notorious improvement in the final results. Despite the simplicity of the CI, the computed form factors and radii are compatible with recent lattice QCD simulations.

DOI: [10.1103/PhysRevD.106.054016](https://doi.org/10.1103/PhysRevD.106.054016)**I. INTRODUCTION**

Quantum chromodynamics (QCD) is regarded as the underlying theory that describes the strong interactions in the Standard Model. This quantum field theory is full of complexities that arise due to its non-Abelian nature, producing very peculiar features in the characterizing running coupling [1], thereby limiting the usage of perturbation theory to certain kinematic regimes [2,3]. Giving this notorious shortcoming, to address several hadron properties and low-energy phenomena, such as confinement and emergent hadronic mass (EHM) [4,5], non-perturbative frameworks turn out to be necessary. For the past few decades, the Dyson-Schwinger equations formalism has proven to be a powerful tool to deal with QCD in the continuum [6,7], paving a traceable connection between the structural properties of hadrons and the fundamental degrees of freedom of QCD, quarks and gluons. Being both a QCD boundstate and a (pseudo) Nambu-Goldstone boson (NGb), the pion takes center stage in our understanding of the strong interactions, specially concerning the nonperturbative phenomena in QCD and EHM [8,9]. Herein, the pion structure is investigated via the computation of form factors (FFs). The pion

vector form factor, namely, the electromagnetic form factor (eFF), describes the coupling of a photon to the pion. It is then directly accessible from experiments [10–21] and investigated through multiple approaches, such as lattice QCD simulations [22–26], Continuum Schwinger Methods (CSM) [27–33] and many other phenomenological approaches [34–41]. Conversely, the pion scalar and tensor form factors, which are not directly accessible as such from experiments, have not received sufficient attention. Notwithstanding, these two form factors still deserve scrutiny. For instance, the scalar form factor (sFF) can be connected with the $\pi\pi$ scattering processes, of extreme relevance in nuclear physics, and can be used to analyze the potentially existing scalar mesons [42]; on the other hand, the calculation of the tensor form factor (tFF) is complementary to explorations concerning gravitational FFs [43,44], and could shed some light in our understanding of the interaction of the pion with higher-spin probes, as it might happen in beyond Standard Model theories. For comprehensive reviews on the pion scalar and tensor FFs, see Refs. [45–52].

In the present work, we calculate the pion scalar, vector and tensor FFs within the DSE approach. Based upon the traditional rainbow-ladder (RL) truncation in QCD [53,54], a modified rainbow-ladder (MRL) truncation is adopted. As detailed in Ref. [55], both truncations preserve the vector and axial-vector Ward-Green-Takahashi identities (WGTIs), ensuring charge conservation and NGb nature of the pion, while also introducing timelike mass poles in the relevant interaction vertices (e.g., a vector meson pole in the quark-photon vertex). The additional structures present in the MRL truncation generate a quark anomalous magnetic

*khepani.raya@dcu.uhu.es

†leichang@nankai.edu.cn

Published by the American Physical Society under the terms of the Creative Commons Attribution 4.0 International license. Further distribution of this work must maintain attribution to the author(s) and the published article's title, journal citation, and DOI. Funded by SCOAP³.

moment (AMM) term, whose impact could be noticeable in meson and baryon FFs [56,57]. The appearance of this term is then desirable and understood as follows: the anomalous chromomagnetic moment for dressed light-quarks, generated nonperturbatively, commensurates (albeit with opposite sign) with its electromagnetic analogue [58,59]. For illustrative purposes, the calculations presented herein are restricted to the symmetry-preserving contact interaction (CI) model introduced in [60,61]. We contrast the results produced in the RL and MRL truncations, observing that, despite the simplicity of the CI, those produced in the MRL case are quite compatible with recent lattice QCD simulations [45].

The manuscript is organized as follows: Section II introduces the CI within the MRL truncation. Section III focuses on the structure and calculation of the relevant interaction vertices: quark-scalar, vector and tensor vertices. Section IV presents the definition and derivation of the pion scalar, vector and tensor FFs. A summary is presented in Sec. V.

II. CONTACT INTERACTION MODEL

Let us now describe the CI model applied to the MRL truncation from Ref. [55] (CI-MRL), which extends the RL case [60] (CI-RL). The DSE for the f -flavored quark propagator, often dubbed as gap equation, reads in the CI model [60]:

$$S_f^{-1}(p) = [i\gamma \cdot p + m_f] + \frac{4}{3m_G^2} \int_q \gamma_\mu S_f(q) \gamma_\mu, \quad (1)$$

where m_f is the Lagrangian current quark mass and $m_G = 0.127$ GeV is an infrared mass scale, the symbol $\int_q := \int d^4q/(2\pi)^4$ denotes a four dimensional Euclidean integral. Note that Eq. (1) possesses a quadratic divergence, such that the integral must be regularized in a Poincaré covariant manner. This implies, first, that a general solution implies a quark propagator written as

$$S_f^{-1}(p) = i\gamma \cdot p + M_f, \quad (2)$$

where M_f is a momentum independent mass function. The gap equation thus becomes

$$M_f = m_f + \frac{M_f}{3\pi^2 m_G^2} \int_0^\infty ds \frac{s}{s + M_f^2}. \quad (3)$$

Using proper time regularization, the integral above is recast as:

$$\frac{1}{s + M_f^2} = \int_0^\infty d\tau e^{-\tau(s + M_f^2)} \rightarrow \int_{\tau_{\text{uv}}}^{\tau_{\text{ir}}} d\tau e^{-\tau(s + M_f^2)}, \quad (4)$$

where τ_{uv} and τ_{ir} are infrared and ultraviolet regulators, respectively. A nonzero value of $\tau_{\text{ir}} := 1/\Lambda_{\text{ir}} = 1/0.24$ GeV⁻¹ ensures the absence of quark production

thresholds, thereby being compatible with confinement. On the other hand, since the contact interaction does not define a renormalizable theory, $\tau_{\text{uv}} := 1/\Lambda_{\text{uv}} = 1/0.905$ GeV⁻¹ cannot be removed and instead plays a dynamical role, setting the scale of all dimensioned quantities. With the regularization prescription we have introduced, the quark mass function is obtained from:

$$M_f = m_f + \frac{M_f}{3\pi^2 m_G^2} C^{iu}(M_f^2), \quad (5)$$

where $C^{iu}(z)/z = \Gamma(-1, z\tau_{\text{uv}}^2) - \Gamma(-1, z\tau_{\text{ir}}^2)$, with $\Gamma(a, z)$ the incomplete Gamma function.

The corresponding meson Bethe-Salpeter equation (BSE) reads:

$$\Gamma_H(P) = -\frac{4}{3m_G^2} \int_q [\gamma_\mu \chi_H(P) \gamma_\mu - \xi \tilde{\Gamma}_j \chi_H(P) \tilde{\Gamma}_j], \quad (6)$$

where $\chi_H(P) = S_f(q) \Gamma_H(P) S_{\bar{f}}(q - P)$, with $\Gamma_H(P)$ being the Bethe-Salpeter amplitude (BSA); H labels the type of meson (encoding Lorentz indices, if any), and P represents the meson total momentum, such that $P^2 = -m_H^2$ (m_H is the meson mass). Note that, setting $\xi = 0$ in Eq. (6), one recovers the CI-RL case. In this way, we will refer as nonladder structures to those that are accompanied by ξ , and those are: $\tilde{\Gamma}_n = \{\mathbb{I}, \gamma_5, \frac{i}{\sqrt{6}} \sigma_{\mu\nu}\}$.

Despite the simplicity of CI, significant features of QCD such as confinement and DCSB are preserved within this framework. Furthermore, the CI is proven to be a reliable tool to the meson and baryon spectra, as well as the electro-weak elastic and transition FFs [55–57,60–69]. From this point on, we will focus on the properties of the pion. The isospin symmetric limit $m_u = m_d$ would be considered, therefore flavor indices shall be omitted for simplicity. The nature of the CI model entails the pion BSA only depends on the total momentum P , such that, a general for of the pion BSA reads

$$\Gamma_\pi(P) = \gamma_5 \left[i E_\pi(P) + \frac{\gamma \cdot P}{M} F_\pi(P) \right]. \quad (7)$$

As explained in Ref. [55], the contributions proportional to ξ in Eq. (6) (dubbed NL terms) can be recast under Fierz transformation as $\frac{1}{3} \sigma_{\alpha\beta} \text{tr}_D [\sigma_{\alpha\beta} \chi_H(P)]$, making apparent that the NL pieces do not contribute in the pseudoscalar and axial-vector channels. Consequently, in the case of the pion, the solutions to the Eq. (6) will be the same in both the CI-RL and CI-MRL cases. However, scalar and vector channels are affected by the NL terms; this would naturally impact the corresponding interaction vertices, as discussed below. In fact, a first effect is observed in the structure acquired by the BSA of the ρ meson [55] which, in the CI-MRL case reads

TABLE I. The model inputs: $m_G = 0.127$ GeV, $\tau_{uv} = 1/0.905$ GeV $^{-1}$, $\tau_{ir} = 1/0.24$ GeV $^{-1}$, and $\xi = 0.6$. The produced masses and pion properties are listed below. The superscript c denotes the BSAs have been canonically normalized [60]. Mass units in GeV.

M	m_π	f_π	m_σ	m_{a1}	m_ρ	E_π^c	F_π^c
$m = 0.007$	0.405	0.139	0.103	0.815	1.131	0.771	3.90
							0.575

$$\Gamma_\mu^p(P) = \gamma_\mu^T(P)E_\rho(P) + \frac{1}{M}\sigma_{\mu\nu}P_\nu F_\rho(P), \quad (8)$$

while in the CI-RL truncation one finds $F_\rho(P) = 0$, so it would be completely defined by the structure

$$\gamma_\mu^T(P) = \gamma_\mu - \frac{\gamma \cdot P}{P^2}P_\mu. \quad (9)$$

With these observations in mind, we fix the model parameters as follows: those already appearing in the CI-RL are fixed in order to reproduce the pion mass and decay constant; on the other hand, the strength of the NL pieces, ξ , will be set to reproduce the mass of the ρ meson. Model inputs, meson masses and other static properties are collected in Table I. In the next section, we discuss about the structure interaction vertices within this approach: quark-scalar (QS), quark-vector (QV) and quark-tensor (QT) vertices.

III. QUARK SCALAR, PHOTON AND TENSOR VERTICES

In principle, a fully covariant description of the interaction vertices (herein QS, QP and QT vertices) might require the latter to be characterized by several tensor structures (e.g., Refs. [33,70–72]). In the CI, the seemingly overwhelming task of sensibly determining each set of structures greatly simplifies due to the momentum independent nature of the model; i.e., the dressing functions accompanying the different tensor structures do not depend on the relative momentum and, therefore, many tensor structures are cancelled by the requirement that its corresponding dressing function be zero. In this way, the QS, QP, and QT vertices can be represented as follows:

$$\begin{aligned} \Gamma^S(Q) &= f_S(Q^2)\mathbb{I}, \\ \Gamma_\mu^V(Q) &= f_{V1}(Q^2)\gamma_\mu^L + f_{V2}(Q^2)\gamma_\mu^T + f_{V3}(Q^2)\frac{\sigma_{\mu\nu}Q_\nu}{M}, \\ \Gamma_{\mu\nu}^T(Q) &= f_{T1}(Q^2)\sigma_{\mu\nu} + f_{T2}(Q^2)\frac{i}{M}(Q\sigma_{\mu\nu} - \sigma_{\mu\nu}Q) \\ &\quad + f_{T3}(Q^2)\frac{i^2}{M^2}Q\sigma_{\mu\nu}Q. \end{aligned} \quad (10)$$

where $\gamma_\mu^T = \gamma_\mu - \frac{Q_\mu}{Q^2}$, $\gamma_\mu^L = \gamma_\mu - \gamma_\mu^T$; $\Gamma^\#(Q) = \{\Gamma^S(Q), \Gamma_\mu^V(Q), \Gamma_{\mu\nu}^T(Q)\}$ denotes the fully dressed QS, QP, and QT vertices, respectively. The vertices satisfy an inhomogeneous BSE, namely:

$$\begin{aligned} \Gamma^\#(Q) &= \gamma^\# - \frac{4}{3m_G^2} \int_q \gamma_\alpha S(q) \Gamma^\#(Q) S(q-Q) \gamma_\alpha \\ &\quad + \frac{4\xi}{3m_G^2} \int_q \tilde{\Gamma}_n S(q) \Gamma^\#(Q) S(q-Q) \tilde{\Gamma}_n. \end{aligned} \quad (11)$$

where the inhomogeneous term $\gamma^\# = \{\mathbb{I}, \gamma_\mu, \sigma_{\mu\nu}\}$ clearly depends on the vertex we are describing. To solve this equation, one inserts Eq. (10) into Eq. (11), projects out the different elements on the basis and takes the corresponding Dirac and color traces. This procedure yields a collection of coupled integral equations for the dressing functions $\{f_S(Q^2), f_{Vi}(Q^2), f_{Ti}(Q^2)\}$, whose solutions are plotted through Figs. (1–3). Some details concerning the QT vertex and the subsequent evaluation of the tFF are found in the Appendix (the steps therein detailed are quite general and can be applied to the rest of the cases).

In solving Eq. (11) for the quark-scalar vertex, one realizes that the profile acquired by $f_S(Q^2)$ turns out to be harder than expected and thus inadequate for a proper description of the sFF. The reason lies within the simple tensor structure acquired by the scalar vertex in the CI framework [a simple identity matrix, Eq. (10)], which prevails in both CI-RL and CI-MRL cases. Thus, when calculating the pion scalar form factor, we use the following monopole Ansatz instead:

$$\bar{f}_S(Q^2) = \frac{1}{1 + Q^2/m_\sigma^2}, \quad (12)$$

where $m_\sigma = 0.815$ GeV is the scalar meson mass computed in the CI-MRL scheme, and which also appears as a timelike mass pole in the actual solution of $f_S(Q^2)$. Figure 1 shows the comparison between the computed

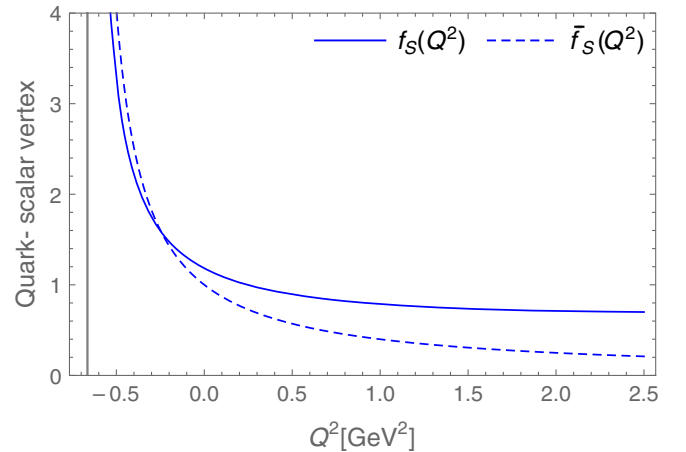


FIG. 1. Quark-scalar vertex dressing function. The solid line is obtained by solving the quark-scalar vertex BSE, Eq. (11), while the dashed line corresponds to the monopole Ansatz from Eq. (12). The vertical line in the timelike region indicates the position of the scalar mass pole, i.e., $Q^2 = -m_\sigma^2$.

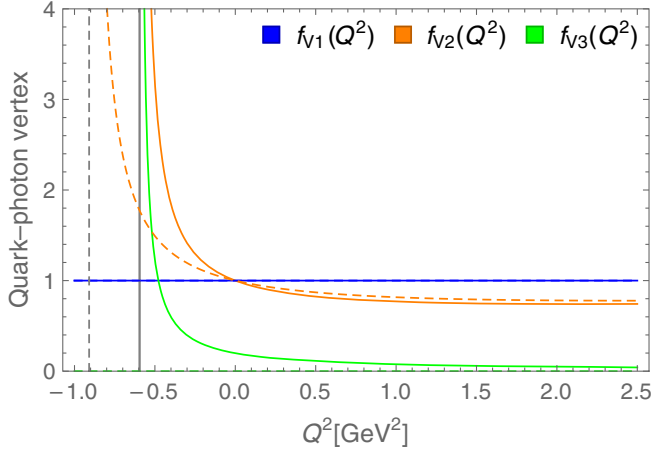


FIG. 2. Quark-photon vertex dressing functions. The blue, orange and green line stands for three dressing functions of the quark-photon vertex defined in Eq. (10). Solid lines corresponds to the CI-MRL case while the dashed lines are obtained in the CI-RL truncation. For each case, the vertical lines in the timelike region denote the indicate of the mass pole of the dressing function $f_{V2}(Q^2)$, i.e., $Q^2 = -m_\rho^2$.

QS dressing function $f_S(Q^2)$ and the monopole Ansatz, $\tilde{f}_S(Q^2)$, from Eq. (12).

The obtained dressing functions of the quark-photon vertex are depicted in Fig. 2. With or without NL pieces appearing in the corresponding Bethe-Salpeter kernel, a trivial solution is found for the longitudinal piece of the vertex, i.e., $f_{V1}(Q^2) = 1$. Appearing in both truncations, $f_{V2}(Q^2)$ features a vector meson pole at $Q^2 = -m_\rho^2$, where the ρ meson mass acquires its physical value ($m_\rho = 0.771$ GeV) in the CI-MRL truncation, as opposed to the CI-RL case in which an inflated mass is obtained instead ($m_\rho = 0.929$ GeV in Ref. [62] and $m_\rho = 0.953$ GeV with our preferred value of m_G). In addition, it is seen that $f_{V2}(Q^2 \rightarrow \infty) \rightarrow 1$, a condition that ensures that the tree level vertex, γ_μ , is faithfully recovered in the large Q^2 limit. The third dressing function, $f_{V3}(Q^2)$, characterizes the Q^2 evolution of the AMM term which, being nonzero only in the CI-MRL case,¹ as a consequence of the richer structure of the Bethe-Salpeter kernel, Eq. (11).

Similarly, for the QT vertex, the CI-MRL truncation also produces 3 independent structures, Eq. (10). The corresponding dressing functions are depicted in Fig. 3. Notably, all of them have a pole at $Q^2 = -m_T^2$, where m_T can be regarded as the mass of some intermediate tensor resonance; within our framework, it happens to coincide with m_ρ . The existence of the NL term in the Bethe-Salpeter kernel decreases the value m_T so that, as in the QP vertex,

¹In some occasions, the AMM term is added by hand in CI-RL related calculations [56,57], adopting a particular the form for $f_{V3}(Q^2)$.

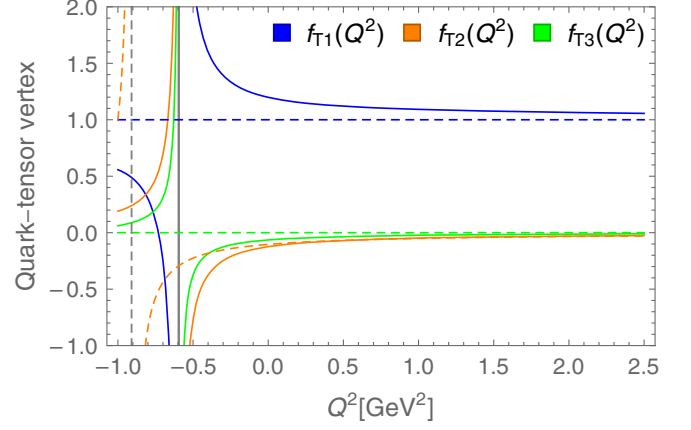


FIG. 3. Quark-tensor vertex dressing functions. The blue, orange and green line stands for three dressing functions of the quark-tensor vertex defined in Eq. (10). Solid lines corresponds to the CI-MRL calculations while the dashed lines are those performed in the CI-RL truncation. For each case, the vertical lines in the timelike region denote the indicate of the mass pole $Q^2 = -m_T^2$.

the position of the pole move closer to $Q^2 = 0$. This means a greater influence of the mass pole in the low Q^2 domain of FFs, which translates into larger charge radii and a softer behavior in the vicinity of $Q^2 = 0$. Taking $\xi = 0$, i.e., the CI-RL case, the quark-tensor vertex dramatically simplifies. There is no longer a pole in the dressing functions $f_{T1,T3}$ and, in fact, those acquire trivial profiles: $f_{T1} = 1$ and $f_{T3} = 0$.

IV. PION SCALAR, VECTOR, AND TENSOR FORM FACTORS

With the quark propagators, pion Bethe-Salpeter amplitude and corresponding interaction vertices at hand, we are now in position to compute the scalar, vector and tensor FFs in the impulse approximation (IA) [32]:

$$T^\#(K, Q)F_\#^\pi(Q^2) = 2\text{tr}_{CD} \int_q \{i\Gamma_\pi(-p_f)S(q+p_f) \times i\Gamma^\#(Q)S(q+p_i)i\Gamma_\pi(p_i)S(q)\}, \quad (13)$$

where tr_{CD} indicates trace over color and Dirac indices. The label $\#$ refers to scalar, vector and tensor cases such that, naturally, $\Gamma^\#$ are the interaction vertices from Eq. (10), while $F_\#$ correspond to the FFs dressing the matrix elements $T^\#(K, Q)$:

$$T^S(K, Q) = i\mathbb{I}, \quad (14)$$

$$T_\mu^V(K, Q) = 2K_\mu, \quad (15)$$

$$T_{\mu\nu}^T(K, Q) = -\frac{K_\mu Q_\nu - K_\nu Q_\mu}{m_\pi}. \quad (16)$$

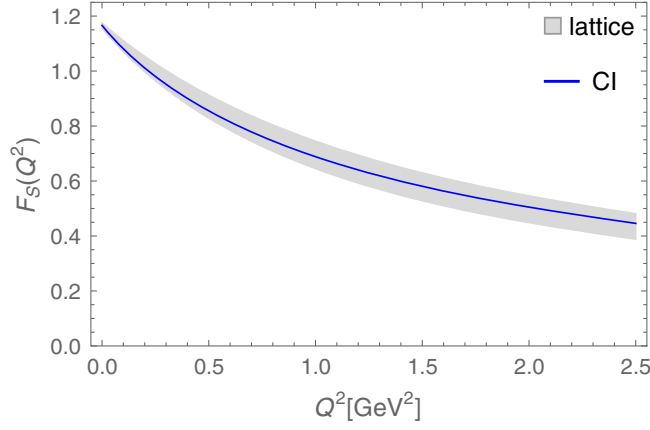


FIG. 4. Pion scalar form factor $F_S^\pi(Q^2)$. The solid line is our computed CI-MRL result, using the vertex dressing from Eq. (12). The band corresponds to the lattice QCD calculation from Ref. [45].

The kinematics is defined as follows: $Q = p_f - p_i$ is the momentum of the incoming gauge boson and $p_{i,f} = K \mp \frac{Q}{2}$ are the incoming and outgoing pion momentum, respectively; on-shell conditions entail $p_{i,f}^2 = -m_\pi^2$, such that $K \cdot Q = 0$ and $K^2 = -m_\pi^2 - \frac{Q^2}{4}$. The key steps in calculation are presented in the Appendix. The computed form factors are displayed in Figs. 4–6.

Our final result for the pion sFF agrees fairly well with that from the lattice calculation in Ref. [45]. A crucial piece for such outcome is the monopole Ansatz for the quark-scalar dressing function, $\bar{f}_S(Q^2)$, given in Eq. (12). If one were to take $f_S(Q^2)$ instead, the actual solution of the corresponding BSE, the very simple structure of Γ_S permitted by the CI model would produce a notoriously harder sFF. This of course could be anticipated from Fig. 1,

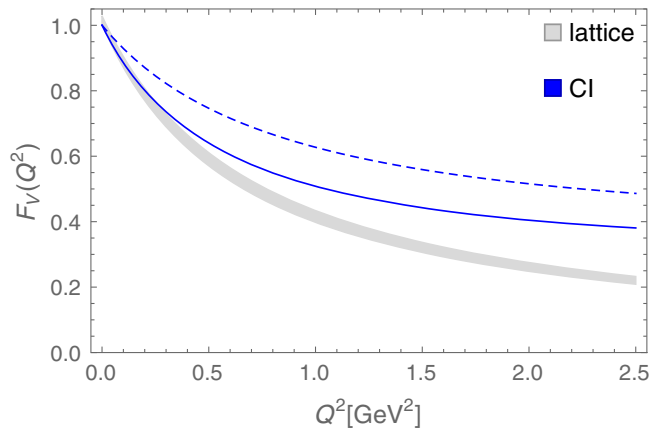


FIG. 5. Pion vector form factor $F_V^\pi(Q^2)$. The solid line corresponds to our result using the CI-MRL truncation, while the dotted line is the analogous for the CI-RL case. The band corresponds to the lattice QCD calculation from Ref. [45].

highlighting the need of an artificial improvement of the quark-scalar vertex within the CI framework.

The vector form factor, namely the electromagnetic form factor, is depicted in Fig. 5. Compared to the CI-RL result, the one obtained from the CI-MRL truncation is suppressed and much closer to the lattice QCD result. The suppressing effect comes, mainly, from the AMM term in the quark-photon vertex, but also due to the smaller computed value of m_ρ , which moves the vector meson pole closer to the spacelike axis and, consequently, produces a larger charge radius. As the momentum transfer increases, the flaws of the CI are exposed and the difference between the CI calculations and lattice QCD becomes larger. In general, one would expect harder form factors to be produced by the CI interaction model [56,57], since the nature of the CI implies constant mass functions and BSAs, which in turn lead to much simpler interaction vertices. In particular for the pion, it is well known that a symmetry-preserving treatment of the CI incorporates a pseudovector component in the pion BSA, Eq. (7), which eventually produces a pion eFF [61] with an asymptotic behavior in marked contradiction with the prescriptions of perturbative QCD [2]; a similar outcome occurs for the pion to two-photon transition form factors [60]. Leaving the hardness issues aside, it is still notorious that, unlike the CI-RL case, our CI-MRL approach produces a vector FF compatible with that obtained from lattice QCD in a low Q^2 region.

In the case of the tFF, the triangle diagram from Eq. (13) is, in principle, insufficient to satisfy the WGTI; namely, charge conservation is not ensured by means of having $Q_\mu T_T^{\mu\nu}(K, Q) \neq 0$. This requires the IA to be completed with other diagrams which turn out to be proportional to $g_{\mu\nu}$; for self-consistency, $\Gamma_{\mu\nu}^T$ in Eq. (10) would also require such completion, ensuring the quark-tensor vertex satisfies a WGTI of its own [73]. Notwithstanding, as discussed in the Appendix, the tFF is decoupled from its matrix element

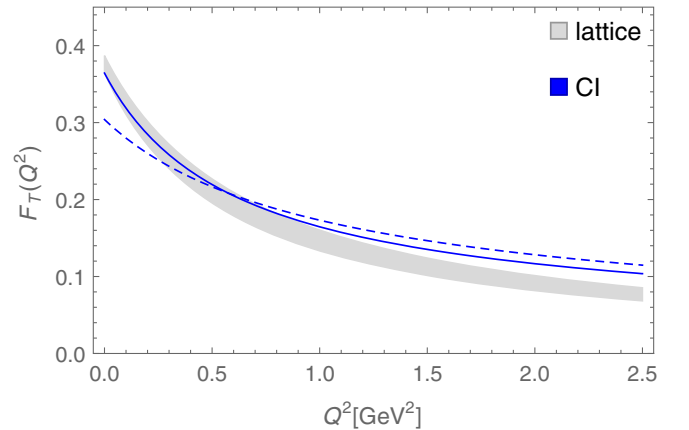


FIG. 6. Pion tensor form factor $F_T^\pi(Q^2)$. The solid line corresponds to our result using the CI-MRL truncation, while the dotted line is the analogous for the CI-RL case. The band corresponds to the lattice QCD calculation from Ref. [45].

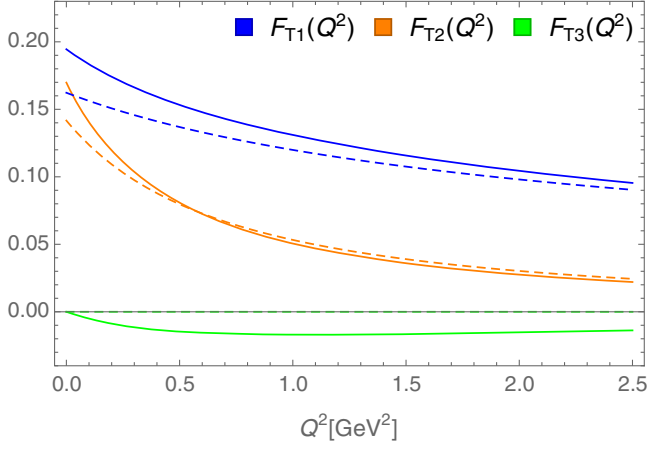


FIG. 7. The ingredients of the form factor from the three structures of the quark-tensor vertex. The solid line is computed using CI-MRL and the dashed line is computed with CI-RL.

after contracting with $K_\mu Q_\nu$; therefore, due to the on-shell condition $K \cdot Q = 0$, any contribution coming from $g_{\mu\nu}$ vanishes. This makes the present approach sufficient for a consistent description of the tFF. Our results in this case are presented in Figs. 6 and 7. The former depicts our final outcomes in the CI-RL and CI-MRL truncations, as compared with those from Ref. [45]; the latter dissects the individual contributions of the QT vertex pieces to the tFF. Focusing on Fig. 6, it is clear that the CI-MRL calculation improves that obtained within CI-RL, producing a tFF in keen agreement with the lattice result over a rather generous domain of Q^2 . Again, there an increasing discrepancy between the CI predictions and lattice simulation is expected as Q^2 becomes larger. To further scrutinize on the impacts of the NL term on the computed tFF, we separate the contributions of each piece of the quark-tensor vertex in Eq. (10) to the tFF,

$$F_T^\pi(Q^2) = F_{T1}^\pi(Q^2) + F_{T2}^\pi(Q^2) + F_{T3}^\pi(Q^2). \quad (17)$$

The individual contributions are depicted in Fig. 7. Capitalizing on $F_{T1,T2}^\pi(Q^2)$, it is clear that the difference between the CI-RL and CI-MRL results is essentially due to the $Q^2 = -m_T^2$ pole. For $F_{T2}^\pi(Q^2)$, the poles are shifted according to the computed value of m_T , while for $F_{T1}^\pi(Q^2)$, the mass pole is completely removed in the CI-RL case. As discussed in Sec. III, the presence of the NL term implies a decreasing in the value of m_T , letting the pole position move closer to $Q^2 = 0$ and, consequently, the form factors $F_{T1,T2}^\pi(Q^2)$ exhibit a steeper falloff in the low Q^2 spacelike domain. Regarding $F_{T3}^\pi(Q^2)$, the third structure characterizing the quark-tensor vertex, $\frac{i^2}{M^2} Q \sigma_{\mu\nu} Q \sim Q^2$, only survives if the NL term appears the corresponding Bethe-Salpeter kernel. Furthermore, the projection operator that decouples the tFF from its matrix element produces a

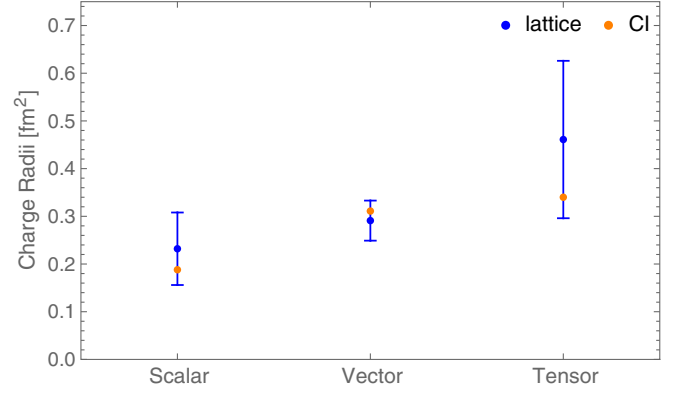


FIG. 8. Scalar, vector and tensor charge radii, as defined in Eq. (18). The orange points corresponds to values obtained within the CI-MRL scheme, while the blue data points are those from lattice QCD [45].

vanishing $F_{T3}^\pi(Q^2)$ at $Q^2 = 0$. Conversely, as Q^2 increases, the CI-MRL obtained form factor $F_T^\pi(Q^2)$ is suppressed mainly because of the negative contribution given by $F_{T3}^\pi(Q^2)$. The destructive interference of $F_{T1,T2}(Q^2)$ with $F_{T3}(Q^2)$ then produces softer behavior at large Q^2 .

For a final comparison, we compute the corresponding charge radii, defined as

$$\langle r^2 \rangle_\# = \left. \frac{6}{F_\#(0)} \frac{\partial F_\#(Q^2)}{\partial Q^2} \right|_{Q^2=0}, \quad (18)$$

and producing the CI-MRL inferred values of:

$$\begin{aligned} r_S^{\pi^2} &= (0.434 \text{ fm})^2, \\ r_V^{\pi^2} &= (0.558 \text{ fm})^2, \\ r_T^{\pi^2} &= (0.583 \text{ fm})^2. \end{aligned} \quad (19)$$

A first thing to notice is the pattern $r_S < r_V \lesssim r_T$, which is indeed is the same followed by the inverse of the masses, i.e., $1/m_\sigma < 1/m_\rho = 1/m_T$. The comparison between the CI-MRL and lattice results are shown in Fig. 8. Since the CI-MRL exhibits comparable values and slopes of the vector and tensor form factors at $Q^2 = 0$, the charge radii are in agreement with lattice QCD simulations. In comparison with traditional CI calculations (for instance, Ref. [62]), the value $r_V^\pi = 0.558 \text{ fm}$ lies closer to the experimental one [74], $r_V^{\pi, \text{exp}} = 0.659(4) \text{ fm}$, and to that from the analysis of Ref [75], $r_V^{\pi, \text{spm}} = 0.640(7) \text{ fm}$. This outcome is a consequence of the richer structure of the quark-photon vertex: roughly, the contribution from the f_{V2} dressing (the one containing the vector meson pole) enhances by 50% that coming from γ_μ alone, while f_{V3} , the AMM piece, further enhances such value by 25%. A similar reasoning could be applied to r_T^π as well, where the $\sigma_{\mu\nu}$ term alone (in the QT vertex) produces a

charge radius about 25% smaller than the one reported in Eq. (19).

V. SUMMARY

In this article, the pion scalar, vector and tensor FFs, as well as the corresponding charge radii, are investigated within a contact interaction model of QCD. Following a previous study in the vector meson sector [55], the Bethe-Salpeter kernel describing the scalar, vector and tensor channels, is complemented with new structures in addition to those coming from the rainbow-ladder truncation alone. Despite this, and just as the CI-RL does, the CI-MRL truncation is consistent with the vector and axial-vector WGTIs. In implementing this truncation, the structure of the quark-vector (quark-photon) and quark-tensor vertices is enriched, with respect to its CI-RL counterpart, and we have seen that this leads to a positive impact on the FFs under study. Comparing the produced FFs with those obtained from recent lattice QCD [45], we can conclude the following:

Even though the momentum independent nature of the CI model produces, typically, harder form factors, the CI-MRL truncation brings some improvements in the Q^2 dependence of such. When computed under the CI-MRL scheme, the scalar, vector and tensor form factors display a better compatibility with the lattice results at spacelike momenta; much better than in the CI-RL case. This is a consequence of the profile that the interaction vertices acquire under this truncation. For instance, the quark-vector (quark-photon) vertex contains an AMM term in addition to the transverse piece containing the vector meson pole.

On the other hand, the QT vertex exhibits a nontrivial profile in the three dressing functions characterizing it; two of them feature a mass pole in the timelike axis, which produces both a larger charge radius and a better behavior at small Q^2 ; a third one, f_{T3} , which is nonzero only in the CI-MRL case, modulates the behavior at large Q^2 in such a way that one obtains a softer tFF, in better agreement with the lattice QCD result. This would imply that for the tFF, the CI-MRL leads to improvements at both small and large

Q^2 . For the scalar case, however, the QS vertex dressing function one obtains from its Bethe-Salpeter equation is not sufficiently damped. This would produce a sFF way too hard, making it necessary to introduce a sensible Ansatz for the vertex dressing function, in order to get a proper description. This crucial drawback is well understood from the very simple structure that the quark-scalar vertex acquires in the CI model, which prevails in both CI-RL and CI-MRL truncations. If computed within the CI-MRL model, all charge radii computed herein are plainly compatible with those from lattice QCD. Contrary to the CI-RL case, the mass of the vector meson can be placed at its physical value, so that the pole impacts the small Q^2 region to a greater extent and, thus enlarging the values of the charge radii. The AMM term appearing in the quark-photon vertex, also plays a positive role in getting a much sensible value for the radii.

Therefore, all virtues of the computed FFs and corresponding charge radii are attributed to the extended structure of the symmetry-preserving CI-MRL truncation, which is also known to significantly improve the description of the static properties and electromagnetic FFs of the ρ meson [55]. Further extensions concerning the axial-vector meson are currently being investigated.

ACKNOWLEDGMENTS

K.R. acknowledges valuable discussions with J. Rodríguez Quintero. Work supported by National Natural Science Foundation of China (Grant No. 12135007).

APPENDIX: QUARK-TENSOR VERTEX AND TENSOR FORM FACTOR

This appendix shows some key steps in the calculation of the dressed quark-tensor vertex and corresponding pion tensor form factor. The steps described herein are quite general and applicable for the rest of the cases.

Let us start from the dressed quark-tensor vertex, which satisfies the following inhomogeneous BSE:

$$\Gamma_{\mu\nu}^T(Q) = \sigma_{\mu\nu} - \frac{4}{3m_G^2} \int_q \gamma_\alpha S(q) \Gamma_{\mu\nu}^T(Q) S(q-Q) \gamma_\alpha + \frac{4\xi}{3m_G^2} \int_q \tilde{\Gamma}_n S(q) \Gamma_{\mu\nu}^T(Q) S(q-Q) \tilde{\Gamma}_n \quad (\text{A1})$$

where $\tilde{\Gamma}_n = \{\mathbb{1}, \gamma_5, \frac{i}{\sqrt{6}} \sigma_{\mu\nu}\}$, and

$$\Gamma_{\mu\nu}^T(Q) = f_{T1}(Q^2) \sigma_{\mu\nu} + f_{T2}(Q^2) \frac{i}{M} (Q\sigma_{\mu\nu} - \sigma_{\mu\nu} Q) + f_{T3}(Q^2) \frac{i^2}{M^2} Q\sigma_{\mu\nu} Q. \quad (\text{A2})$$

Using the above equation, the main idea is to conveniently recast Eq. (A1) as follows:

$$\begin{pmatrix} f_{T1}(Q^2) \\ f_{T2}(Q^2) \\ f_{T3}(Q^2) \end{pmatrix} = \begin{pmatrix} a_{11} & a_{12} & a_{13} \\ a_{21} & a_{22} & a_{23} \\ a_{31} & a_{32} & a_{33} \end{pmatrix} \begin{pmatrix} f_{T1}(Q^2) \\ f_{T2}(Q^2) \\ f_{T3}(Q^2) \end{pmatrix} + \begin{pmatrix} 1 \\ 0 \\ 0 \end{pmatrix} \quad (\text{A3})$$

Because the three basis elements of $\Gamma_{\mu\nu}^T(Q)$ are Dirac-trace orthogonal, we can easily calculate the matrix entries $a_{i,j}$. In fact, it is sufficient to multiply Eq. (A1) by each element from the basis in Eq. (A2). For instance, one has:

$$\begin{aligned} a_{22} &= \text{tr}_{CD} \left\{ \frac{\not{Q}\sigma_{\mu\nu} - \sigma_{\mu\nu}\not{Q}}{72m_G^2 Q^2} \left[\int_q \gamma_\alpha S(q) (\not{Q}\sigma_{\mu\nu} - \sigma_{\mu\nu}\not{Q}) S(q-Q) \gamma_\alpha - \int_q \xi \tilde{\Gamma}_n S(q) (\not{Q}\sigma_{\mu\nu} - \sigma_{\mu\nu}\not{Q}) S(q-Q) \tilde{\Gamma}_n \right] \right\} \\ &= \frac{4}{3m_G^2} \int_0^1 d\alpha \int_q \frac{q^2 - 2\alpha(1-\alpha)Q^2 + 2M^2}{(q^2 + \alpha(1-\alpha)Q^2 + M^2)^2}, \end{aligned} \quad (\text{A4})$$

where the second line has been obtained after a combination of Feynman parametrization and changes of variables. Then, one can choose whether to use the axial-vector WGTI [60], in order to get rid of the integral involving a q^2 in the numerator. As a matter of fact, it is not necessary for the 4-momentum integrals concerning the quark-scalar vertex, but it is quite convenient in the vector and tensor cases. In particular, still for a_{22} , one gets:

$$a_{22} = -Q^2 \tilde{I}(Q^2), \quad (\text{A5})$$

where the following definitions have been employed:

$$\tilde{I}(Q^2) = \frac{1}{3\pi^2 m_G^2} \int_0^1 \alpha(1-\alpha) \tilde{C}_1^{iu}(\omega(\alpha, Q^2)) d\alpha, \quad (\text{A6})$$

$$\tilde{C}_1^{iu}(\omega) = -\frac{d}{d\omega} C^{iu}(\omega), \quad (\text{A7})$$

$$\omega(\alpha, Q^2) = \alpha(1-\alpha)Q^2 + M^2. \quad (\text{A8})$$

Proceeding analogously with the rest of the coefficients a_{ij} , one obtains the following expressions for the quark-tensor vertex dressing functions:

$$\begin{aligned} f_{T1}(Q^2) &= \frac{-3(\xi M^2 Q^2 I(Q^2)^2 - 4\xi M^2 Q^2 I(Q^2) \tilde{I}(Q^2) - 4\xi M^2 I(Q^2) + 6Q^2 I(Q^2) + 6)}{2(2\xi M^2 I(Q^2) + 2\xi Q^2 \tilde{I}(Q^2) - 3)[(1 + Q^2 \tilde{I}(Q^2))(-2\xi M^2 I(Q^2) + 2\xi Q^2 \tilde{I}(Q^2) + 3) + \xi M^2 Q^2 I(Q^2)^2]}, \\ f_{T2}(Q^2) &= \frac{-3M^2 I(Q^2)}{4[(1 + Q^2 \tilde{I}(Q^2))(-2\xi M^2 I(Q^2) + 2\xi Q^2 \tilde{I}(Q^2) + 3) + \xi M^2 Q^2 I(Q^2)^2]}, \\ f_{T3}(Q^2) &= \frac{3\xi M^2 (M^2 I(Q^2)^2 + 4Q^2 \tilde{I}(Q^2)^2 + 4\tilde{I}(Q^2))}{2(2\xi M^2 I(Q^2) + 2\xi Q^2 \tilde{I}(Q^2) - 3)[(1 + Q^2 \tilde{I}(Q^2))(-2\xi M^2 I(Q^2) + 2\xi Q^2 \tilde{I}(Q^2) + 3) + \xi M^2 Q^2 I(Q^2)^2]}, \end{aligned} \quad (\text{A9})$$

where

$$I(Q^2) = \frac{1}{3\pi^2 m_G^2} \int_0^1 \tilde{C}_1^{iu}(\omega(\alpha, Q^2)) d\alpha. \quad (\text{A10})$$

To get the tFF from its matrix element, we now multiply both left- and right-hand sides of Eq. (13) by $K_\mu Q_\nu$, such that

$$\begin{aligned} -\frac{K^2 Q^2}{m_\pi} F_V^\pi(Q^2) &= 2\text{tr}_{CD} \int_q \left\{ i\Gamma_\pi(-p_f) S(q+p_f) i \left[f_{T1}(Q^2) i\mathbf{K}\not{Q} + f_{T2}(Q^2) \frac{2Q^2 \mathbf{K}}{M} + f_{T3}(Q^2) \frac{iQ^2 \mathbf{K}\not{Q}}{M^2} \right] \right. \\ &\quad \left. \times S(q+p_i) i\Gamma_\pi(p_i) S(q) \right\} \end{aligned} \quad (\text{A11})$$

Given the structure of the pion BSA, Eq. (7), the tensor form factor can be split in three parts: one proportional to $(E_\pi^c)^2$, an analogous for $(F_\pi^c)^2$, and a third one containing the crossed term $E_\pi^c F_\pi^c$. In this case, the one with $(F_\pi^c)^2$ can be evaluated directly, while the other two requires some algebraic manipulations to ensure the axial WGTI and translational invariance in the CI [60]. For instance, the following expression accompanies the $(E_\pi^c)^2$ term:

$$\begin{aligned} & \frac{8N_c m_\pi}{M(m_\pi^2 + Q^2/4)} \int_q \frac{(m_\pi^2 + Q^2/4)(M^2 f_{T1}(Q^2) - 4(q^2 + M^2) f_{T2}(Q^2) + Q^2 f_{T3}(Q^2)) + 8(K \cdot q)(q^2 + M^2 - m_\pi^2) f_{T2}(Q^2)}{((q + K + Q/2)^2 + M^2)((q + K - Q/2)^2 + M^2)(q^2 + M^2)} \\ &= \frac{8N_c m_\pi}{M(m_\pi^2 + Q^2/4)} \int_q \left[\frac{-4(m_\pi^2 + Q^2/4 - 2(K \cdot q)) f_{T2}(Q^2)}{((q + K + Q/2)^2 + M^2)((q + K - Q/2)^2 + M^2)} \right. \\ & \quad \left. + \frac{(m_\pi^2 + Q^2/4)(M^2 f_{T1}(Q^2) + Q^2 f_{T3}(Q^2)) - 8(K \cdot q) m_\pi^2 f_{T2}(Q^2)}{((q + K + Q/2)^2 + M^2)((q + K - Q/2)^2 + M^2)(q^2 + M^2)} \right] \end{aligned} \quad (\text{A12})$$

As with the QT vertex, from a combination of Feynman parametrization and changes of variables, it is possible to evaluate each addend separately. For the crossed term of $E_\pi^c F_\pi^c$, we follow a similar approach. Finally, one arrives at:

$$\begin{aligned} F_T^\pi(Q^2) &= \frac{N_c m_\pi}{2\pi^2 M^3} \left\{ E_\pi^c [M^2 F_\pi^c f_{T1}(Q^2) + 2M^2(2F_\pi^c - E_\pi^c) f_{T2}(Q^2) + Q^2 f_{T3}(Q^2)] \int_0^1 d\alpha \bar{C}_1^{iu}(\omega(\alpha, Q^2)) \right. \\ & \quad - 2F_\pi^c \int_0^1 du_1 \int_0^{1-u_1} du_2 [M^2(E_\pi^c + F_\pi^c) f_{T1}(Q^2) + ((3u_1 + 3u_2 - 2)m_\pi^2 + (u_1 + u_2)Q^2) F_\pi^c f_{T2}(Q^2) \\ & \quad + Q^2(E_\pi^c + F_\pi^c) f_{T3}(Q^2)] \bar{C}_1^{iu}(\omega'(u_1, u_2, Q^2)) \\ & \quad + 2 \int_0^1 du_1 \int_0^{1-u_1} du_2 [(M^2 E_\pi^{c2} + (2M^2 + (u_1 + u_2)m_\pi^2) F_\pi^{c2} \\ & \quad + (-3M^2 + (3u_1^2 + 2u_1(3u_2 - 1) + u_2(3u_2 - 2))m_\pi^2 + 3u_1 u_2 Q^2) E_\pi^c F_\pi^c) (M^2 f_{T1}(Q^2) + Q^2 f_{T3}(Q^2)) \\ & \quad + (-2(u_1 + u_2)m_\pi^2 M^2 E_\pi^{c2} + 2M^2(2m_\pi^2 - (u_1 + u_2)Q^2) E_\pi^c F_\pi^c \\ & \quad + (u_1 u_2 (u_1 + u_2) Q^4 + (u_1 + u_2 - 1)(u_1 + u_2)^2 m_\pi^4 + (5u_1 + 5u_2 - 6)m_\pi^2 M^2 + 3(u_1 + u_2) Q^2 M^2 \\ & \quad \left. + (-u_1^3 + u_1^2(6u_2 + 1) + 2u_1 u_2(3u_2 - 2) - u_2^2(u_2 - 1)) m_\pi^2 Q^2) F_\pi^{c2}] f_{T2}(Q^2)] \bar{C}_2^{iu}(\omega'(u_1, u_2, Q^2)) \right\} \end{aligned} \quad (\text{A13})$$

where

$$\bar{C}_2^{iu}(\omega) = \frac{1}{2} \frac{d^2}{d\omega^2} C^{iu}(\omega) \quad (\text{A14})$$

$$\omega'(u_1, u_2, Q^2) = M^2 + m_\pi^2(u_1 + u_2)(u_1 + u_2 - 1) + u_1 u_2 Q^2 \quad (\text{A15})$$

-
- [1] Z.-F. Cui, J.-L. Zhang, D. Binosi, F. de Soto, C. Mezrag, J. Papavassiliou, C. D. Roberts, J. Rodríguez-Quintero, J. Segovia, and S. Zafeiropoulos, Effective charge from lattice QCD, *Chin. Phys. C* **44**, 083102 (2020).
- [2] G. P. Lepage and S. J. Brodsky, Exclusive processes in perturbative quantum chromodynamics, *Phys. Rev. D* **22**, 2157 (1980).
- [3] A. V. Efremov and A. V. Radyushkin, Factorization and asymptotical behavior of pion form-factor in QCD, *Phys. Lett.* **94B**, 245 (1980).
- [4] C. D. Roberts, Empirical consequences of emergent mass, *Symmetry* **12**, 1468 (2020).
- [5] C. D. Roberts, D. G. Richards, T. Horn, and L. Chang, Insights into the emergence of mass from studies of pion and kaon structure, *Prog. Part. Nucl. Phys.* **120**, 103883 (2021).
- [6] C. D. Roberts and A. G. Williams, Dyson-Schwinger equations and their application to hadronic physics, *Prog. Part. Nucl. Phys.* **33**, 477 (1994).
- [7] C. S. Fischer, QCD at finite temperature and chemical potential from Dyson-Schwinger equations, *Prog. Part. Nucl. Phys.* **105**, 1 (2019).
- [8] T. Horn and C. D. Roberts, The pion: An enigma within the Standard Model, *J. Phys. G* **43**, 073001 (2016).

- [9] J. Arrington *et al.*, Revealing the structure of light pseudoscalar mesons at the electron-ion collider, *J. Phys. G* **48**, 075106 (2021).
- [10] S. R. Amendolia *et al.* (NA7 Collaboration), A measurement of the spacelike pion electromagnetic form-factor, *Nucl. Phys.* **B277**, 168 (1986).
- [11] C. J. Bebek *et al.*, Electroproduction of single pions at low epsilon and a measurement of the pion form-factor up to $q^2 = 10\text{-GeV}^2$, *Phys. Rev. D* **17**, 1693 (1978).
- [12] L. M. Barkov *et al.*, Electromagnetic pion form-factor in the timelike region, *Nucl. Phys.* **B256**, 365 (1985).
- [13] C. J. Bebek, C. N. Brown, M. Herzlinger, S. D. Holmes, C. A. Lichtenstein, F. M. Pipkin, S. Raither, and L. K. Sistrerson, Measurement of the pion form-factor up to $q^2 = 4\text{-GeV}^2$, *Phys. Rev. D* **13**, 25 (1976).
- [14] A. Quenzer *et al.*, Pion form-factor from 480-MeV to 1100-MeV, *Phys. Lett.* **76B**, 512 (1978).
- [15] D. Bisello *et al.* (DM2 Collaboration), The pion electromagnetic form-factor in the timelike energy range $1.35\text{-GeV} \leq \sqrt{s} \leq 2.4\text{-GeV}$, *Phys. Lett. B* **220**, 321 (1989).
- [16] S. R. Amendolia *et al.*, Measurement of the pion form-factor in the timelike region for q^2 values between $.1\text{-GeV}/c^2$ and $.18\text{-GeV}/c^2$, *Phys. Lett.* **138B**, 454 (1984).
- [17] V. M. Aul'chenko *et al.* (CMD-2 Collaboration), Measurement of the pion form-factor in the range 1.04-GeV to 1.38-GeV with the CMD-2 detector, *JETP Lett.* **82**, 743 (2005).
- [18] R. R. Akhmetshin *et al.* (CMD-2 Collaboration), High-statistics measurement of the pion form factor in the rho-meson energy range with the CMD-2 detector, *Phys. Lett. B* **648**, 28 (2007).
- [19] J. Volmer *et al.* (Jefferson Lab F(pi) Collaboration), Measurement of the Charged Pion Electromagnetic Form-Factor, *Phys. Rev. Lett.* **86**, 1713 (2001).
- [20] T. Horn *et al.* (Jefferson Lab F(pi)-2 Collaboration), Determination of the Charged Pion Form Factor at $Q^2 = 1.60$ and $2.45\text{-}(\text{GeV}/c)^2$, *Phys. Rev. Lett.* **97**, 192001 (2006).
- [21] G. M. Huber *et al.* (Jefferson Lab Collaboration), Charged pion form-factor between $Q^2 = 0.60\text{-GeV}^2$ and 2.45-GeV^2 . II. Determination of, and results for, the pion form-factor, *Phys. Rev. C* **78**, 045203 (2008).
- [22] H. B. Meyer, Lattice QCD and the Timelike Pion Form Factor, *Phys. Rev. Lett.* **107**, 072002 (2011).
- [23] R. Frezzotti, V. Lubicz, and S. Simula (ETM Collaboration), Electromagnetic form factor of the pion from twisted-mass lattice QCD at $N(f) = 2$, *Phys. Rev. D* **79**, 074506 (2009).
- [24] P. A. Boyle, J. M. Flynn, A. Juttner, C. Kelly, H. P. de Lima, C. M. Maynard, C. T. Sachrajda, and J. M. Zanotti, The Pion's electromagnetic form-factor at small momentum transfer in full lattice QCD, *J. High Energy Phys.* **07** (2008) 112.
- [25] X. Feng, S. Aoki, S. Hashimoto, and T. Kaneko, Timelike pion form factor in lattice QCD, *Phys. Rev. D* **91**, 054504 (2015).
- [26] X. Gao, N. Karthik, S. Mukherjee, P. Petreczky, S. Syritsyn, and Y. Zhao, Pion form factor and charge radius from lattice QCD at the physical point, *Phys. Rev. D* **104**, 114515 (2021).
- [27] A. Miramontes, A. Bashir, K. Raya, and P. Roig, Pion and Kaon box contribution to $a_\mu\text{HLbL}$, *Phys. Rev. D* **105**, 074013 (2022).
- [28] A. S. Miramontes, H. Sanchis Alepuz, and R. Alkofer, Elucidating the effect of intermediate resonances in the quark interaction kernel on the timelike electromagnetic pion form factor, *Phys. Rev. D* **103**, 116006 (2021).
- [29] G. Eichmann, C. S. Fischer, E. Weil, and R. Williams, Single pseudoscalar meson pole and pion box contributions to the anomalous magnetic moment of the muon, *Phys. Lett. B* **797**, 134855 (2019); **799**, 135029(E) (2019).
- [30] M. Chen, M. Ding, L. Chang, and C. D. Roberts, Mass-dependence of pseudoscalar meson elastic form factors, *Phys. Rev. D* **98**, 091505 (2018).
- [31] L. Chang, I. C. Cloët, C. D. Roberts, S. M. Schmidt, and P. C. Tandy, Pion Electromagnetic form Factor at Spacelike Momenta, *Phys. Rev. Lett.* **111**, 141802 (2013).
- [32] P. Maris and P. C. Tandy, The pi, K^+ , and K^0 electromagnetic form-factors, *Phys. Rev. C* **62**, 055204 (2000).
- [33] P. Maris and P. C. Tandy, The quark photon vertex and the pion charge radius, *Phys. Rev. C* **61**, 045202 (2000).
- [34] F. Guerrero and A. Pich, Effective field theory description of the pion form-factor, *Phys. Lett. B* **412**, 382 (1997).
- [35] A. P. Bakulev, K. Passek-Kumericki, W. Schroers, and N. G. Stefanis, Pion form-factor in QCD: From nonlocal condensates to NLO analytic perturbation theory, *Phys. Rev. D* **70**, 033014 (2004); **70**, 079906(E) (2004).
- [36] S. J. Brodsky and G. F. de Teramond, Light-front dynamics and AdS/QCD correspondence: The pion form factor in the space- and time-like regions, *Phys. Rev. D* **77**, 056007 (2008).
- [37] K. Ghorbani, Chiral and volume extrapolation of pion and kaon electromagnetic form factor within SU(3) ChPT, *Chin. J. Phys.* **51**, 920 (2013).
- [38] D. Djukanovic, J. Gegelia, A. Keller, S. Scherer, and L. Tiator, Vector form factor of the pion in chiral effective field theory, *Phys. Lett. B* **742**, 55 (2015).
- [39] B. Ananthanarayan, I. Caprini, and D. Das, Test of analyticity and unitarity for the pion form-factor data around the ρ resonance, *Phys. Rev. D* **102**, 096003 (2020).
- [40] S. Cheng, A. Khodjamirian, and A. V. Rusov, Pion light-cone distribution amplitude from the pion electromagnetic form factor, *Phys. Rev. D* **102**, 074022 (2020).
- [41] M. A. Martin Contreras, E. Folco Capossoli, D. Li, A. Vega, and H. Boschi-Filho, Pion form factor from an AdS deformed background, *Nucl. Phys.* **B977**, 115726 (2022).
- [42] S. Dubnicka, A. Z. Dubnickova, R. Kamiński, and A. Liptaj, Pion scalar form factor with correct mass and width of scalar mesons $f_0(500)$ and $f_0(980)$, *Phys. Rev. D* **94**, 054036 (2016).
- [43] A. Freese and I. C. Cloët, Gravitational form factors of light mesons, *Phys. Rev. C* **100**, 015201 (2019).
- [44] J.-L. Zhang, Z.-F. Cui, J. Ping, and C. D. Roberts, Contact interaction analysis of pion GTMDs, *Eur. Phys. J. C* **81**, 6 (2021).
- [45] C. Alexandrou, S. Bacchio, I. Cloet, M. Constantinou, J. Delmar, K. Hadjiyiannakou, G. Koutsou, C. Lauer, and A. Vaquero (ETM Collaboration), Scalar, vector, and tensor form factors for the pion and kaon from lattice QCD, *Phys. Rev. D* **105**, 054502 (2022).
- [46] V. Gülpers, G. von Hippel, and H. Wittig, Scalar pion form factor in two-flavor lattice QCD, *Phys. Rev. D* **89**, 094503 (2014).

- [47] T. Kaneko *et al.* (JLQCD, TWQCD Collaborations), Pion vector and scalar form factors with dynamical overlap quarks, *Proc. Sci. LATTICE2008* (**2008**) 158 [arXiv:0810.2590].
- [48] I. Caprini, Model-independent constraint on the pion scalar form factor and light quark masses, *Phys. Rev. D* **98**, 056008 (2018).
- [49] J. A. Oller and L. Roca, Scalar radius of the pion and zeros in the form factor, *Phys. Lett. B* **651**, 139 (2007).
- [50] T. Hannah, Pion scalar form-factor and the sigma meson, *Phys. Rev. D* **60**, 017502 (1999).
- [51] S. Aoki *et al.* (JLQCD, TWQCD Collaborations), Pion form factors from two-flavor lattice QCD with exact chiral symmetry, *Phys. Rev. D* **80**, 034508 (2009).
- [52] D. Brömmel *et al.* (QCDSF, UKQCD Collaborations), The Spin Structure of the Pion, *Phys. Rev. Lett.* **101**, 122001 (2008).
- [53] A. Bender, C. D. Roberts, and L. Von Smekal, Goldstone theorem and diquark confinement beyond rainbow ladder approximation, *Phys. Lett. B* **380**, 7 (1996).
- [54] H. J. Munczek, Dynamical chiral symmetry breaking, Goldstone's theorem and the consistency of the Schwinger-Dyson and Bethe-Salpeter equations, *Phys. Rev. D* **52**, 4736 (1995).
- [55] Z. Xing, K. Raya, and L. Chang, Quark anomalous magnetic moment and its effects on the ρ meson properties, *Phys. Rev. D* **104**, 054038 (2021).
- [56] K. Raya, L. X. Gutiérrez-Guerrero, A. Bashir, L. Chang, Z. F. Cui, Y. Lu, C. D. Roberts, and J. Segovia, Dynamical diquarks in the $\gamma^{(*)}\mathbf{p} \rightarrow N(1535)\frac{1}{2}^-$ transition, *Eur. Phys. J. A* **57**, 266 (2021).
- [57] D. J. Wilson, I. C. Cloet, L. Chang, and C. D. Roberts, Nucleon and Roper electromagnetic elastic and transition form factors, *Phys. Rev. C* **85**, 025205 (2012).
- [58] L. Chang, Y.-X. Liu, and C. D. Roberts, Dressed-Quark Anomalous Magnetic Moments, *Phys. Rev. Lett.* **106**, 072001 (2011).
- [59] A. Bashir, R. Bermudez, L. Chang, and C. D. Roberts, Dynamical chiral symmetry breaking and the fermion-gauge-boson vertex, *Phys. Rev. C* **85**, 045205 (2012).
- [60] H. L. L. Roberts, C. D. Roberts, A. Bashir, L. X. Gutierrez-Guerrero, and P. C. Tandy, Abelian anomaly and neutral pion production, *Phys. Rev. C* **82**, 065202 (2010).
- [61] L. X. Gutierrez-Guerrero, A. Bashir, I. C. Cloet, and C. D. Roberts, Pion form factor from a contact interaction, *Phys. Rev. C* **81**, 065202 (2010).
- [62] H. L. L. Roberts, A. Bashir, L. X. Gutierrez-Guerrero, C. D. Roberts, and D. J. Wilson, π and ρ mesons, and their diquark partners, from a contact interaction, *Phys. Rev. C* **83**, 065206 (2011).
- [63] H. L. L. Roberts, L. Chang, I. C. Cloet, and C. D. Roberts, Masses of ground and excited-state hadrons, *Few-Body Syst.* **51**, 1 (2011).
- [64] C. Chen, L. Chang, C. D. Roberts, S. Wan, and D. J. Wilson, Spectrum of hadrons with strangeness, *Few-Body Syst.* **53**, 293 (2012).
- [65] J. Segovia, C. Chen, I. C. Cloët, C. D. Roberts, S. M. Schmidt, and S. Wan, Elastic and transition form factors of the $\Delta(1232)$, *Few-Body Syst.* **55**, 1 (2014).
- [66] F. E. Serna, B. El-Bennich, and G. a. Krein, Charmed mesons with a symmetry-preserving contact interaction, *Phys. Rev. D* **96**, 014013 (2017).
- [67] L. X. Gutiérrez-Guerrero, G. Paredes-Torres, and A. Bashir, Mesons and baryons: Parity partners, *Phys. Rev. D* **104**, 094013 (2021).
- [68] R. J. Hernández-Pinto, M. Bedolla-Hernández, L. X. Gutiérrez-Guerrero, and A. Bashir, Elastic meson form factors in a unified scheme, *Rev. Mex. Fis. Suppl.* **3**, 0308106 (2022).
- [69] H.-Y. Xing, Z.-N. Xu, Z.-F. Cui, C. D. Roberts, and C. Xu, Heavy + heavy and heavy + light pseudoscalar to vector semileptonic transitions, arXiv:2205.13642.
- [70] A. S. Miramontes and H. Sanchis-Alepuz, On the effect of resonances in the quark-photon vertex, *Eur. Phys. J. A* **55**, 170 (2019).
- [71] L. Albino, A. Bashir, L. X. G. Guerrero, B. E. Bennich, and E. Rojas, Transverse Takahashi identities and their implications for gauge independent dynamical chiral symmetry breaking, *Phys. Rev. D* **100**, 054028 (2019).
- [72] A. Krassnigg and M. Blank, A covariant study of tensor mesons, *Phys. Rev. D* **83**, 096006 (2011).
- [73] R. Brout and F. Englert, Gravitational ward identity and the principle of equivalence, *Phys. Rev.* **141**, 1231 (1966).
- [74] P. Zyla *et al.* (Particle Data Group), Review of particle physics, *Prog. Theor. Exp. Phys.* **2020**, 083C01 (2020).
- [75] Z.-F. Cui, D. Binosi, C. D. Roberts, and S. M. Schmidt, Pion charge radius from pion + electron elastic scattering data, *Phys. Lett. B* **822**, 136631 (2021).